



Article

An Efficient Cyan Emission from Copper (II) Complexes with Mixed Organic Conjugate Ligands

Jingjing Wang^{1,†}, Junjie Ren^{1,†}, Qinglin Tang¹, Xinzhi Wang¹, Yao Wang¹, Yanxin Wang¹, Zhonglin Du¹, Wei Wang¹, Linjun Huang¹, Laurence A. Belfiore^{1,2} and Jianguo Tang^{1,*}

- ¹ Institute of Hybrid Materials, National Center of International Joint Research for Hybrid Materials Technology, National Base of International Sci. & Tech. Cooperation on Hybrid Materials, Qingdao University, 308 Ningxia Road, Qingdao 266071, China; w1834089@163.com (J.W.); m2019025747@163.com (J.R.); a15666920912@163.com (Q.T.); wangxinzhi1988123@163.com (X.W.); wangyaoqdu@126.com (Y.W.); yanxin_2008@126.com (Y.W.); duzhonglin@qdu.edu.cn (Z.D.); wangwei040901@163.com (W.W.); huanglinjun@qdu.edu.cn (L.H.); belfiore@engr.colostate.edu (L.A.B.)
- ² Department of Chemical and Biological Engineering, Colorado State University, Fort Collins, CO 80523, USA
- * Correspondence: tang@qdu.edu.cn; Tel.: +86-532-85951961
- † Both Jingjing Wang and Junjie Ren have the same contribution to this work.

Abstract: Copper (II) complexes containing mixed ligands were synthesized in dimethyl formamide (DMF). The intense cyan emission at an ambient temperature is observed for solid copper (II) complexes with salicylic acid and a 12% quantum yield with a fluorescent lifetime of approximately 10 ms. Hence, copper (II) complexes with salicylic acid are excellent candidates for photoactive materials. Fourier transform infrared spectroscopy (FTIR) and X-ray photoelectron spectroscopy (XPS) reveal that the divalent copper metal centers coordinate with the nitrogen and oxygen lone pairs of conjugate ligands. XPS binding energy trends for core electrons in lower-lying orbitals are similar for all three copper (II) complexes: nitrogen 1s and oxygen 1s binding energies increase relative to those for undiluted ligands, and copper 2p_{3/2} binding energies decrease relative to that for CuCl₂. The thermal behavior of these copper complexes reveals that the thermal stability is characterized by the following pattern: Cu(1,10-phenanthroline)(salicylic acid) > Cu(1,10-phenanthroline)(2,2'-bipyridine) > Cu(1,10-phenanthroline)(1-benzylimidazole)₂.

Keywords: copper (II) complex; luminescent materials; benzylimidazole; bipyridine; salicylic acid; spectroscopy



Citation: Wang, J.; Ren, J.; Tang, Q.; Wang, X.; Wang, Y.; Wang, Y.; Du, Z.; Wang, W.; Huang, L.; Belfiore, L.A.; et al. An Efficient Cyan Emission from Copper (II) Complexes with Mixed Organic Conjugate Ligands. *Materials* **2022**, *15*, 1719. <https://doi.org/10.3390/ma15051719>

Academic Editor: Wiesław Stręk

Received: 22 January 2022

Accepted: 20 February 2022

Published: 25 February 2022

Publisher's Note: MDPI stays neutral with regard to jurisdictional claims in published maps and institutional affiliations.



Copyright: © 2022 by the authors. Licensee MDPI, Basel, Switzerland. This article is an open access article distributed under the terms and conditions of the Creative Commons Attribution (CC BY) license (<https://creativecommons.org/licenses/by/4.0/>).

1. Introduction

Transition metal ions and complexes have attracted much attention due to their incompletely occupied d-orbitals and highly ordered solid-state structures [1]. These complexes possess unique optical and magnetic properties arising from unpaired d-electrons and a non-zero spin angular momentum. Although some examples of complexes with high-spin ground states and ordered structures have been achieved (Mn) [2–5], the rational design and synthesis of novel transition metal complexes remains a challenge for luminescent sensors, photo-luminescent devices, and biological probes [6–9].

To date, a variety of noble metal complexes have been developed (mainly Au, Ag, and Pt) [10–13] due to their chemical stability and facile synthetic procedures. However, the commercial development of noble metal ions requires further consideration because of their toxic environmental impact. The applications of transition metal complexes exhibit limitations due to the cost of these precious metals and their toxicity. Compared to noble metal s(Au, Ir, and Ru), divalent copper is relatively abundant [14,15], significantly cheaper, has a high thermal stability [16–18], and is readily available from commercial sources. Hence, Cu²⁺ complexes appear to be excellent candidates for this research investigation.

The electronic configuration of divalent copper ions is $[\text{Ar}]3d^9$ or $[\text{Ar}]4s^13d^8$, with incompletely filled d-orbitals and relatively low-energy d-d transitions. Luminescent emission occurs if radiative pathways exist from the excited state to the ground state with a significant quantum yield. However, the free-ion excited states of Cu^{2+} experience ultra-fast non-radiative processes, such that Cu^{2+} complexes are not advantageous from a photo-physical point of view [19]. Due to the influence of organic ligands that quench emission, the luminescent studies of Cu^{2+} complexes are very scarce in the research literature [20–22]. Hence, this investigation of Cu^{2+} complexes, with a high quantum yield, is very challenging. Recently, successful research on copper (II) luminescence has revealed that phenanthroline (i.e., phen) is a promising ligand that does not quench emission [23–25]. The most common preparation method for Cu^{2+} complexes is via the self-assembly of the metal ion center with the appropriate organic ligands to promote the formation of extended framework structures [25,26]. Hence, current research focuses on the synthesis of copper (II) complexes with extended organic frameworks. Organic ligands that contain oxygen or nitrogen donors play important roles in the construction of coordination complexes [27,28]. Previous luminescent results for copper (II) complexes, and their main photo-physical parameters, are listed in Table 1 [25,29,30]. These results provide guidelines for future research on copper (II) complexes that exhibit luminescent emissions with a significant quantum yield and measurable lifetimes. This research investigation extends the results in Table 1 to copper (II) complexes that contain bidentate organic conjugate ligands.

Table 1. Published quantum yield lifetimes and peak emission wavelengths (nm) of Cu^{2+} complexes.

No.	Formula	Quantum Yield (%)	Lifetime (μs)	Peak Emission Wavelength (nm)	Ref.
1	$[\text{Cu}_2(\text{opdc})_2(\text{phen})_2]_n$	2.1	7.2×10^{-4}	450	[25]
2	$[\text{Cu}(\text{bipy})(\text{acac})(\text{NO}_3)]$	3.09	9.05	465	[29]
3	$[\text{Cu}(\text{bipy})(\text{DMF})(\text{NO}_3)_2]$	2.17	5.22	465	[29]
4	$[\text{Cu}(\text{bipy})(\text{Ala})(\text{NO}_3)(\text{H}_2\text{O})]$	3.14	11.2	468	[29]
5	$\text{Cu}(\text{CDHPBC})$	4.0	–	522	[31]

Unlike luminescent emission in trivalent lanthanide complexes, Cu^{2+} emission wavelengths are influenced strongly by the electron donating/withdrawing ability of ligands in the first-shell coordination sphere, as well as organic conjugate ligands, solvents, crystal structures, and pH levels. As indicated in Table 1, visible emission occurs in the range from 450 nm (i.e., blue) to 522 nm (i.e., green). The ligand choice and structure provides some control with respect to copper (II) emission wavelengths in solid-state fluorescent studies.

Combining structural and luminescent factors, the primary objective of this research investigation is to obtain an enhanced blue-green emission of copper (II) complexes that contain favorable conjugate ligands with a light-harvesting ligand-to-metal energy transfer. Previous research in our laboratory focused on several metal–ligand frameworks based on nitrogen- and oxygen-containing organic ligands for lanthanide emission [8,32]. In this investigation of copper (II) emission, the following three Cu^{2+} complexes were designed and synthesized in DMF: A = $\text{Cu}(\text{phen})(\text{bim})_2$, B = $\text{Cu}(\text{phen})(\text{bipy})$, and C = $\text{Cu}(\text{phen})(\text{SA})$, where bim = 1-benzylimidazole, bipy = 2,2'-bipyridine, SA = salicylic acid, and phen = 1,10-phenanthroline. Results presented herein demonstrate that the appropriate design strategies can deliver new phenanthroline-based materials for their use as luminescent materials. In the DMF solution, these complexes emit a cyan color with a significant quantum yield. From an application viewpoint, the cyan emission spectra overlap with carotene absorption [33]. β -carotene is a key compound in grain plants, fruit trees, and other key food resource plants, which absorb solar energy at wavelengths between 500 nm and 550 nm. Hence, the significance for agricultural harvest improvement is very important.

2. Materials and Methods

2.1. Chemicals

All analytical reagents were purchased from commercial sources and used without further purification. The details are as follows: 1-benzylimidazole (bim), 2,2'-bipyridyl (bipy), salicylic acid (SA), the antenna co-ligand 1,10-phenanthroline (phen), and analytical grade solvent *N,N*-dimethylformide (DMF) were purchased from Aladdin (Shanghai, China). Copper chloride dehydrate ($\text{CuCl}_2 \cdot 2\text{H}_2\text{O}$) (98%) was purchased from R&M Chemical (Shanghai, China).

2.2. Material Preparation

Synthesis of Complex A: $\text{Cu}(\text{bim})_2(\text{phen})$. Complex A was prepared via a mixture of $\text{CuCl}_2 \cdot 2\text{H}_2\text{O}$ (17 mg, 0.10 mmol), bim (31 mg, 0.20 mmol), whose structure of the bim is as shown in Figure 1a, and phen (19 mg, 0.10 mmol) in 5 mL of DMF, which was stirred for 6 h at 30 °C. A dark blue turbid liquid was then obtained after 6 h and it was centrifuged to obtain the desired material. The structure of Complex A is shown in Figure 1d. The elemental analysis (%) and calc (exp) for Complex A is: C 65.56 (67.72), Cl 11.83 (6.26), N 12.75 (14.81), Cu 9.86 (11.2), and yield (63%, 32.76 mg). The IR (cm^{-1}): (C=N: 1429 cm^{-1} , Cu-N: 510 cm^{-1}). From Figure 2a, the ^1H NMR spectrum of Complex A in DMSO-*d*₆ solution confirms its structure. The imidazole protons generally give a signal between 7.8 and 8.1 ppm in DMSO solution.

Synthesis of Complex B: $\text{Cu}(\text{bipy})(\text{phen})$. Complex B was synthesized via the same procedure as Complex A, except that 1-benzylimidazole was replaced by 2,2'-bipyridyl with the structure shown in Figure 1b. A dark blue turbid liquid was then obtained after 6 h and it was centrifuged to obtain the desired material. The structure of the Complex B is shown in Figure 1e. The elemental analysis (%) and calc (exp) for Complex B is: C 52.71 (58.09), Cl 19.51 (15.63), N 12.06 (12.32), Cu 15.72 (13.97), and yield (38%, 25.46 mg). The IR (cm^{-1}): (C=N: 1416 cm^{-1} , Cu-N: 435 cm^{-1}). Figure 2 reveals that the ^1H NMR spectrum of Complex B exhibits a signal at between 7.9 and 8.1 ppm in DMSO solution.

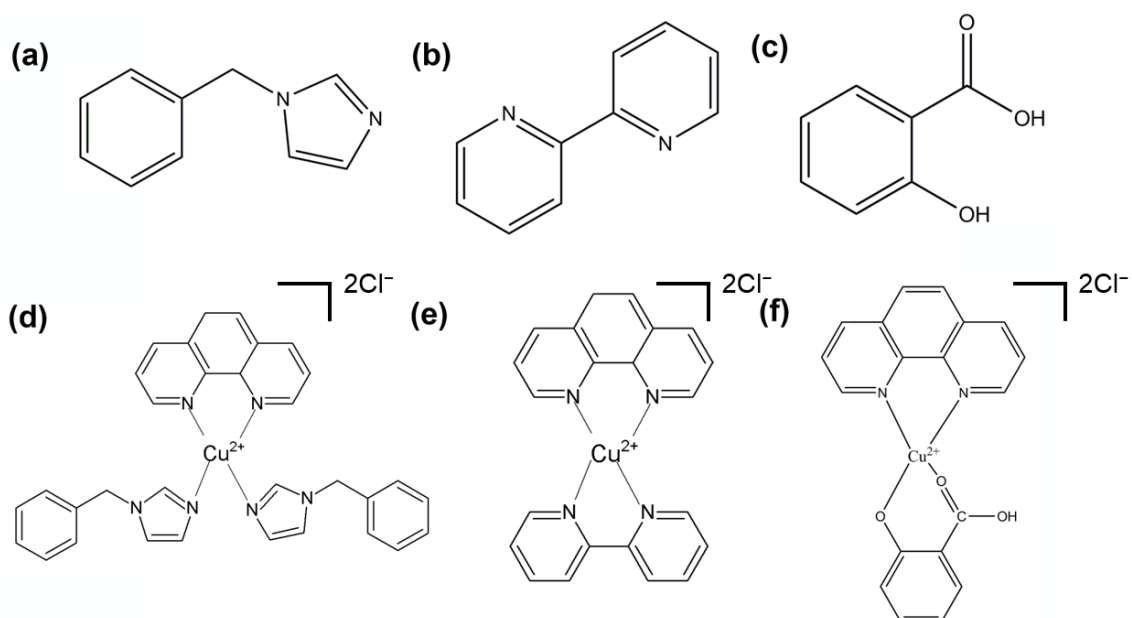


Figure 1. Structural chemical formulae of the three ligands (a–c) and its complexes (d–f).

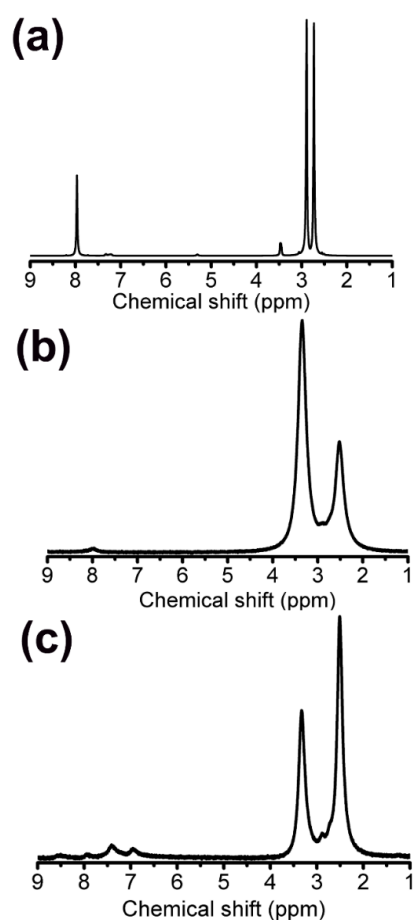


Figure 2. ^1H NMR of copper (II) complexes with (a) benzylimidazole, (b) bipyridine, and (c) salicylic acid. The concentration of all copper (II) complexes in NMR experiments is 10 mM.

Synthesis of Complex C: Cu(SA)(phen). Complex C was also synthesized via the same procedure as Complex A, except that 1-benzylimidazole was replaced by salicylic acid with the structure shown in Figure 1c. A dark blue turbid liquid was then obtained after 6 h and it was centrifuged to obtain the desired material. The structure of the Complex C is shown in Figure 1f. The elemental analysis (%) and calc (exp) for Complex C is: C 50.07 (52), Cl 21.76 (16.19), N 10.84 (6.38), Cu 16.73 (14.48), O 0.6 (10.95), and yield (76%, 38 mg). The IR (cm^{-1}): (C=N: 1416 cm^{-1} , Cu-N: 487 cm^{-1} Cu-O: 432 cm^{-1}). Figure 2 reveals that the hydroxyl proton NMR signal of salicylic acid is observed at a larger chemical shift (i.e., 6.8–7.5 ppm) because hydrogen bonding affects this resonance in Complex C.

2.3. Characterization

Infrared spectra were recorded on a Perkin Elmer 400 Fourier transform spectrometer (FTIR) between $4000\text{--}400\text{ cm}^{-1}$. The ^1H NMR spectra were measured in DMSO-*d*₆ solutions on the Bruker Av HD 400 spectrophotometer (400 MHz), using TMS as an internal reference. XPS spectra were obtained by a XSAM-800 Kratos spectrometer. Al ($K\alpha$ at 1486.6 eV) or Mg ($K\alpha$) radiation was used to excite photoelectrons from Cu ($2p_{3/2}$), O (1s), and N (1s) core levels. The UV–Vis spectra were measured on a UV755B (Shanghai Youke Instrument Co., Ltd., Shanghai, China) spectrophotometer at an ambient temperature. The redox potentials $E_{\text{pCuII/CuI}}$ were measured in the presence of the CHI-832 electrochemical workstation in 0.1 M KCl by using it as a supporting electrolyte for these complexes (0.02 M aqueous solutions). The voltage was scanned from -0.65 to 0.5 V with a scan rate of 100 mVs^{-1} , with glassy carbon, Pt foil, and Ag/AgCl as working, auxiliary, and reference electrodes, respectively. Fluorescent absorption and emission spectra were measured on a Cary Eclipse fluorescence spectrophotometer (Varian, San Francisco, CA, USA) at an

ambient temperature. A thermo-gravimetric analysis (SII TG/DTA 6300) was carried out using a Perkin Elmer TGA 4000 thermogravimetric analyzer. Emission scanning electron microscopy (SEM) images and energy dispersive X-ray (EDX) mapping were recorded on a JSM-6700F field emission scanning microscope (FEI, Czech, The Netherlands).

Figure 3 is a schematic diagram of the coordination of three different copper (II) complexes. All three copper complexes have two kinds of ligands. The first is the co-ligand: phen, and then the species of the second ligand is changed, which is (a) benzylimidazole, (b) bipyridine, and (c) salicylic acid, thereby forming three new copper (II) complexes.

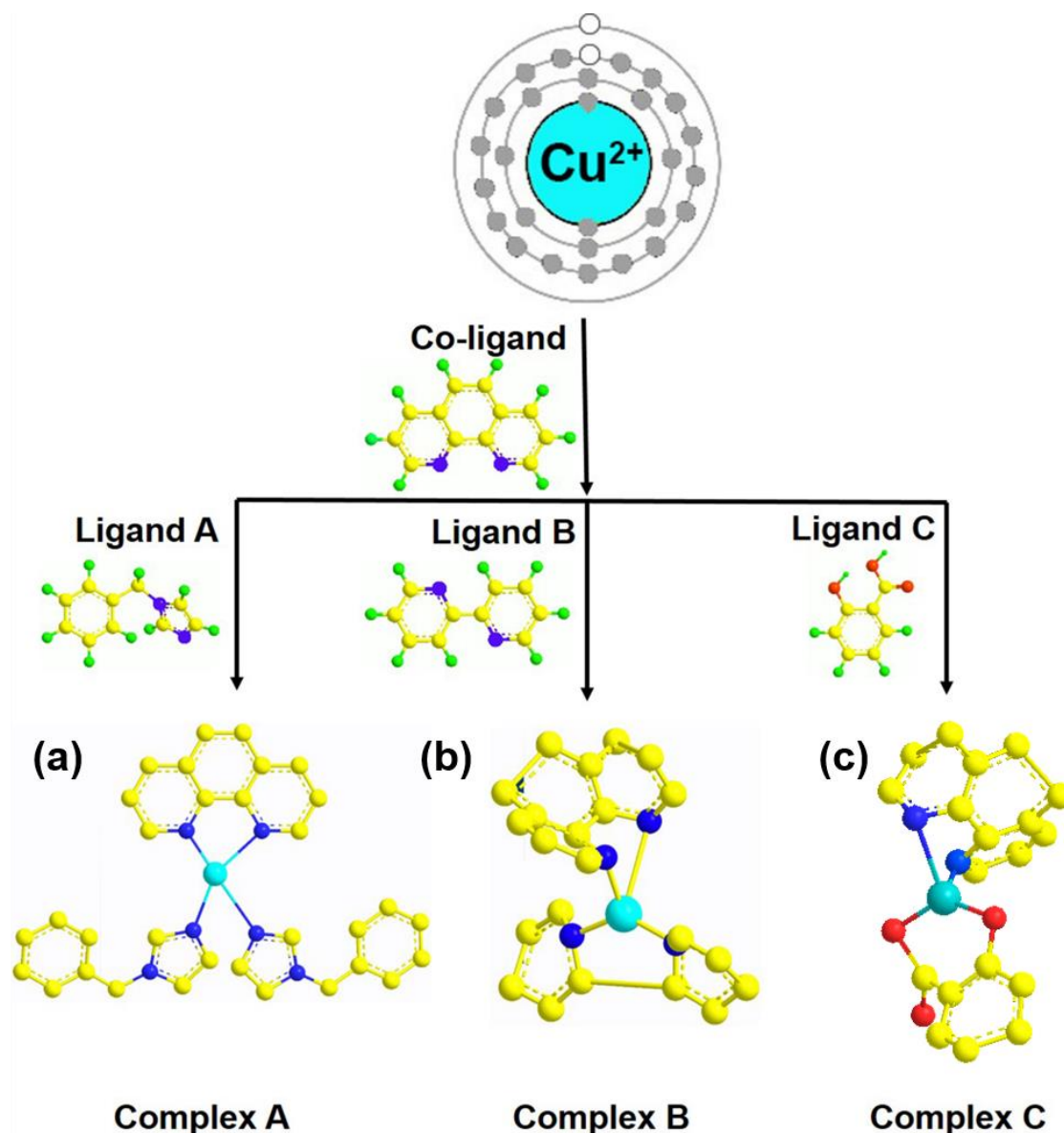


Figure 3. Schematic diagram of copper (II) complexes with (a) benzylimidazole, (b) bipyridine, and (c) salicylic acid.

3. Results and Discussion

3.1. Structures of the Coordination Complexes

The metal–ligand binding in copper (II) complexes was probed via infrared spectra for free ligands and complexes from 400 to 4000 cm^{-1} . The data in Figure 4 reveal that the infrared spectra of three copper (II) complexes are similar to those of the corresponding ligands. The main infrared features in Figure 4 are due to absorptions of benzylimidazole

(spectra 4a), bipyridine (spectra 4b), and the carbonyl group of salicylic acid (spectra 4c). There are some significant shifts in absorption frequencies of important ligand functional groups when these ligands coordinate with copper (II). For example, the imidazole C=N stretch absorbs at 1429 cm^{-1} (upper spectrum in 4a), representing a 12 cm^{-1} shift to a lower frequency in the copper (II) complex with benzylimidazole. This is attributed to copper (II) coordination with the imidazole nitrogen lone pair. In spectra 4b, the carbon–nitrogen in-plane stretch of bipyridine at 1442 cm^{-1} shifts to 1416 cm^{-1} , possibly due to bidentate chelation with copper (II), as illustrated in Figure 4 for Complex B. Copper (II) complexes, with salicylic acid in spectra 4c, reveal a weak shift of the carbonyl stretch from 1658 cm^{-1} to 1652 cm^{-1} , suggesting that the bonding strength of these copper (II) complexes varies as follows: bipyridine > benzylimidazole > salicylic acid. New infrared absorptions for all three copper (II) complexes near 500 cm^{-1} are not observed when copper (II) is absent. For example, copper (II)–nitrogen bonding is probably responsible for the 510 cm^{-1} absorption in complexes with benzylimidazole (spectra 3a), 435 cm^{-1} absorption in complexes with bipyridine (spectra 2b), and the 432 cm^{-1} absorption in complexes with salicylic acid (spectra 4c). The copper (II)–oxygen stretch at 487 cm^{-1} in the upper spectrum of Figure 3c suggests that the carboxylic acid group of salicylic acid coordinates with copper (II) in a bidentate fashion [26,31], as illustrated in Figure 4 for Complex C.

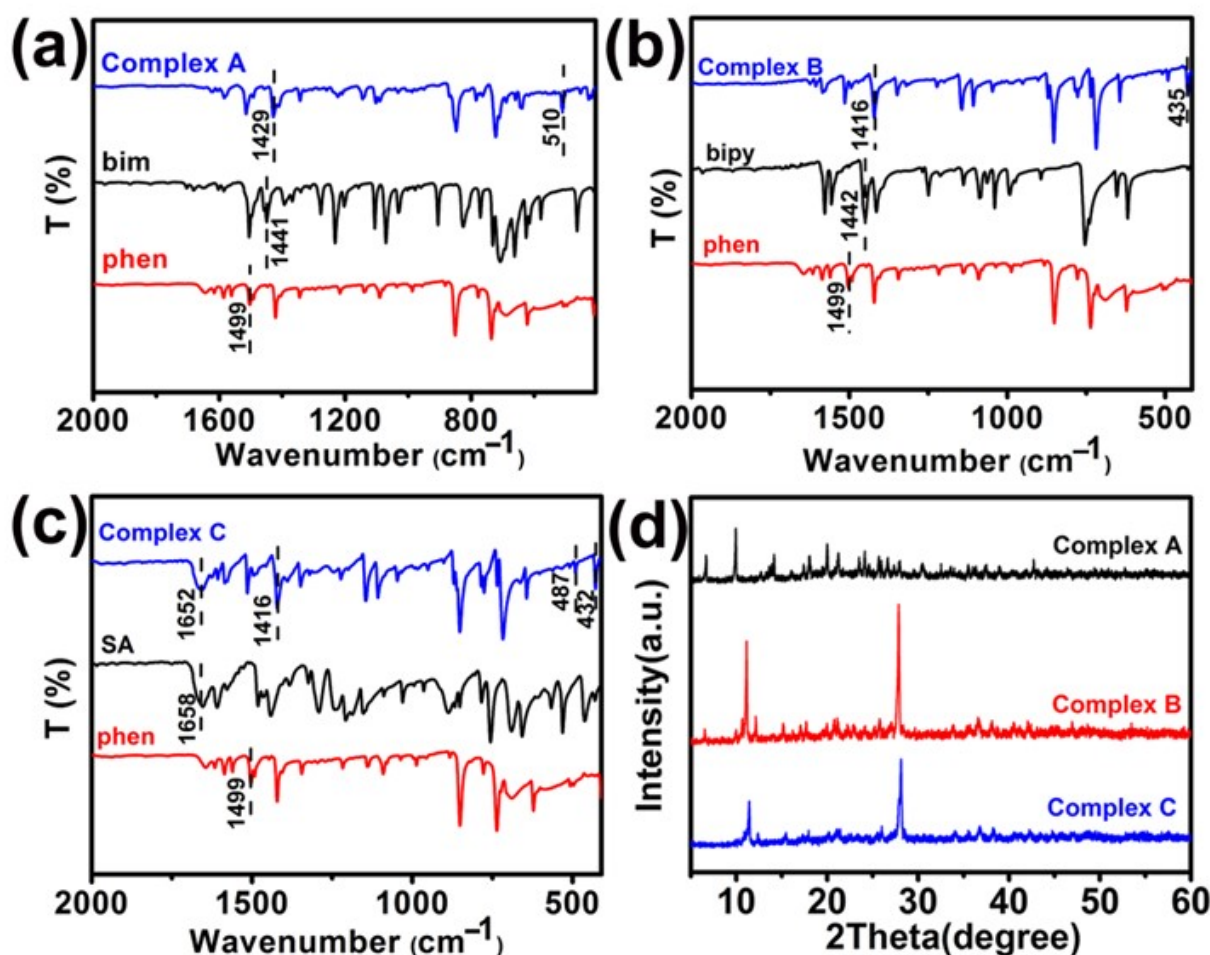


Figure 4. Illustration of FTIR spectra of copper (II) complexes with (a) benzylimidazole, (b) bipyridine, (c) salicylic acid, and (d) X-ray diffractograms of all three complexes using incident radiation at 1.54 \AA .

X-ray diffractograms of the three copper (II) complexes in Figure 4d suggest the formation of a well-defined crystal structure in each case. Diffractograms in Figure 4d were measured from $2\theta = 5^\circ$ to 60° . The strongest reflection for copper (II) complexes

with benzylimidazole (i.e., upper X-ray diffractogram of Figure 4d) occurs at $2\theta \approx 11^\circ$, corresponding to an inter-planar lattice spacing of ≈ 8.8 Å. Two strong Bragg reflections are observed for copper (II) complexes with bipyridine (i.e., the middle X-ray diffractogram of Figure 4d) and salicylic acid (i.e., the lower X-ray diffractogram of Figure 4d) at essentially the same scattering angles in each case: $2\theta \approx 11^\circ$ and 28° , corresponding to the inter-planar lattice spacings of 8.0 Å and 3.2 Å, respectively.

X-ray photoelectron spectroscopy (XPS) yields information about metal–ligand interactions in these copper (II) complexes. Core electron binding energies for nitrogen 1s, oxygen 1s, and copper 2p_{3/2} are illustrated in Figure 5 for all three copper (II) complexes.

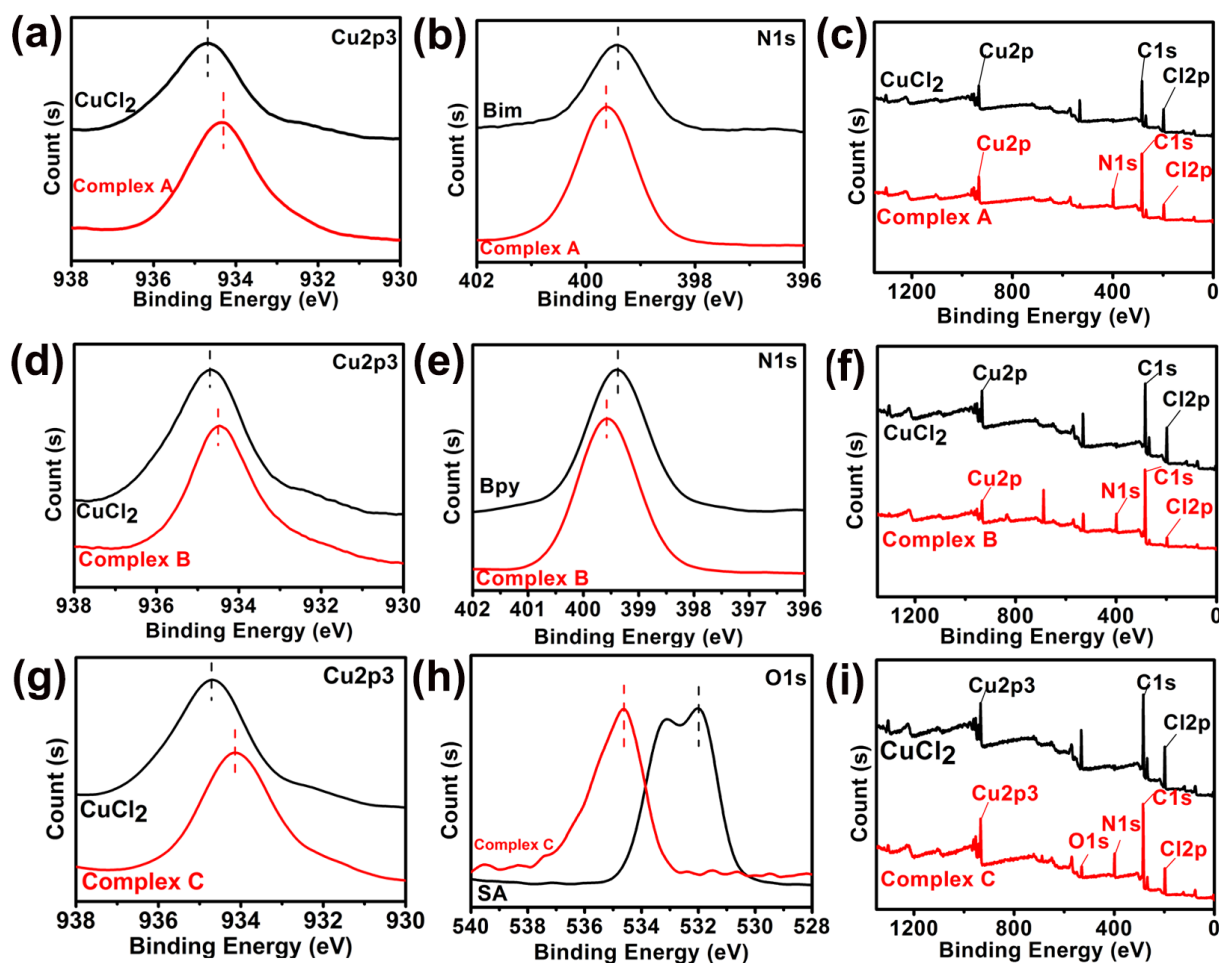


Figure 5. XPS data for Complex A: (a) copper 2p_{3/2}, (b) nitrogen 1s, (c) XPS survey; Complex B: (d) copper 2p_{3/2}, (e) nitrogen 1s, (f) XPS survey; Complex C: (g) copper 2p_{3/2}, (h) oxygen 1s, (i) XPS survey.

Nitrogen 1s binding energies in copper (II) complexes with benzylimidazole are 0.25 eV higher (i.e., 399.57 eV vs. 399.32 eV) relative to those in undiluted benzylimidazole, as illustrated in Figure 5b. A slightly smaller but similar shift in nitrogen 1s binding energies is observed in copper (II) complexes with bipyridine (i.e., 399.57 eV vs. 399.42 eV), according to Figure 5e. In copper (II) complexes with salicylic acid, oxygen 1s binding energies are 1.50 eV higher (i.e., 534.62 eV vs. 533.12 eV), relative to those in undiluted salicylic acid, as illustrated in Figure 5h. Two different oxygen 1s binding energies are resolved in Figure 5h for undiluted salicylic acid, but they are not resolved in the copper (II) complex. For all three copper (II) complexes investigated herein, the higher intensity peak for copper 2p_{3/2} electrons near 935 eV, due to spin-orbit coupling, reveals that binding energies are 0.20 eV to 0.55 eV smaller than the copper 2p_{3/2} binding energy of CuCl₂ (i.e., 934.67 eV) according

to Figure 5a,d,g. The copper 2p_{3/2} binding energies are the largest for bipyridine complexes (i.e., 934.47 eV) in Figure 5d and the smallest for salicylic acid complexes (i.e., 934.12 eV) in Figure 5g. XPS binding energy trends for core electrons in lower-lying orbitals are similar for all three copper (II) complexes: nitrogen 1s and oxygen 1s binding energies increase relative to those for undiluted ligands, and copper 2p_{3/2} binding energies decrease relative to that for CuCl₂ [34–36].

A SEM analysis reveals that the ligand coordination with Cu²⁺ considerably modifies the surface morphology of the three complexes. STEM and EDX mapping images of prepared Cu²⁺ complexes are presented in Figure 6, demonstrating that N (green), O (yellow), and Cu (purple) elements are homogeneously distributed throughout the surface layer. This observation suggests that, in the vicinity of the surface layer, Cu²⁺ coordinates with all of the ligands employed in this study [37]. From Table 2, the content of each element in the complex is seen.

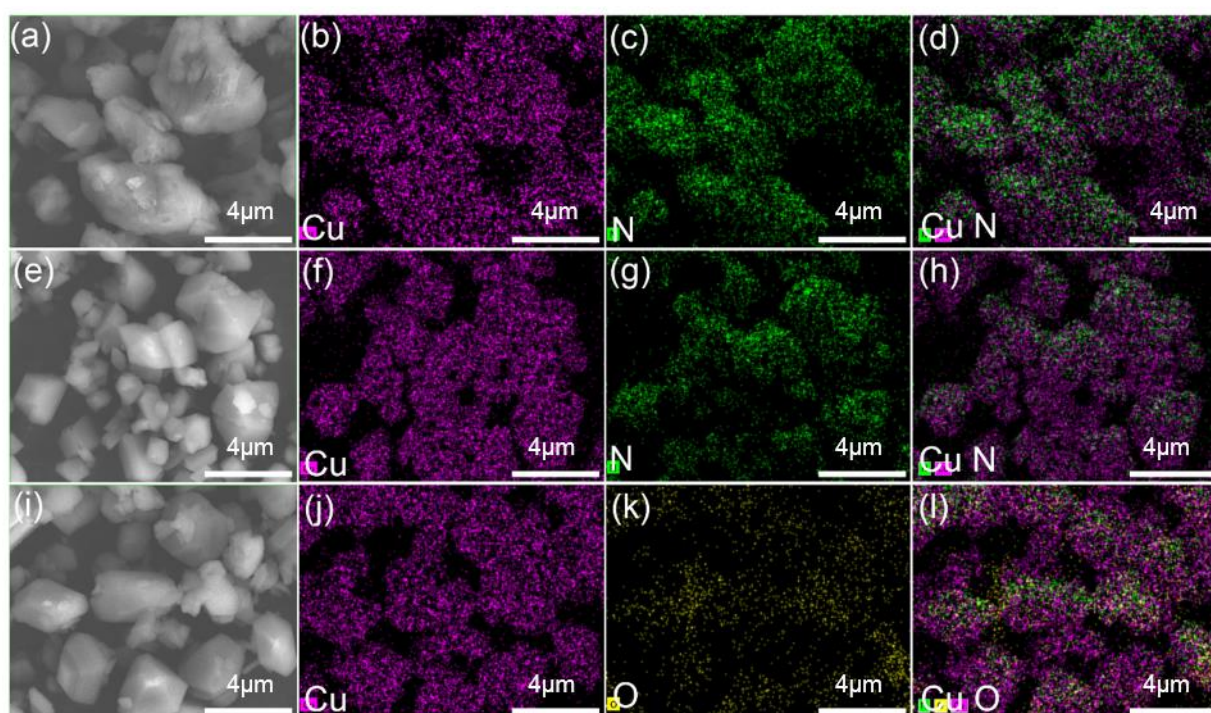


Figure 6. STEM dark-field (DF) images (a) SEM image of Complex A, (b–d) elemental mapping of Cu and N, (e) SEM image of Complex B, (f–h) elemental mapping of Cu and N, (i) SEM image of Complex C, (j–l) elemental mapping of Cu and O.

Table 2. The elemental analysis of the copper complexes.

	Complex A		Complex B		Complex C	
	Mass Norm. (%)	Atom (%)	Mass Norm. (%)	Atom (%)	Mass Norm. (%)	Atom (%)
Copper	9.86	2.26	15.72	4.09	16.73	4.49
Nitrogen	12.75	13.28	12.06	14.24	10.84	13.21
Carbon	65.56	79.59	52.71	72.57	50.07	71.17
Chlorine	11.83	4.86	19.51	9.1	21.76	10.48
Oxygen	—	—	—	—	0.6	0.64

The content of each element in the complexes can be seen from Table 2. The element of the complexes contains copper, nitrogen, and oxygen.

3.2. Fluorescent Behavior of the Complexes

Figure 7 illustrates the absorption spectra of important undiluted ligands and all three copper (II) complexes in DMF at an ambient temperature. According to Figure 7a,b, prominent asymmetric absorption bands exhibit maxima at 280 nm and 294 nm, respectively, for π - π^* electronic excitations in benzylimidazole and bipyridine. There is a slight shift of these absorptions to a lower energy when benzylimidazole and bipyridine are coordinated with copper (II), according to the red curves in Figure 7a,b. Similarly, for salicylic acid complexes with copper (II) in Figure 7c, there is a broad asymmetric absorption for the undiluted ligand at 286 nm with components of this absorption band at a lower energy in the copper (II) complex. Phenomenologically, there exists minor red-shifts for all three absorption bands in the presence of copper (II), according to the red curves in Figure 7a–c.

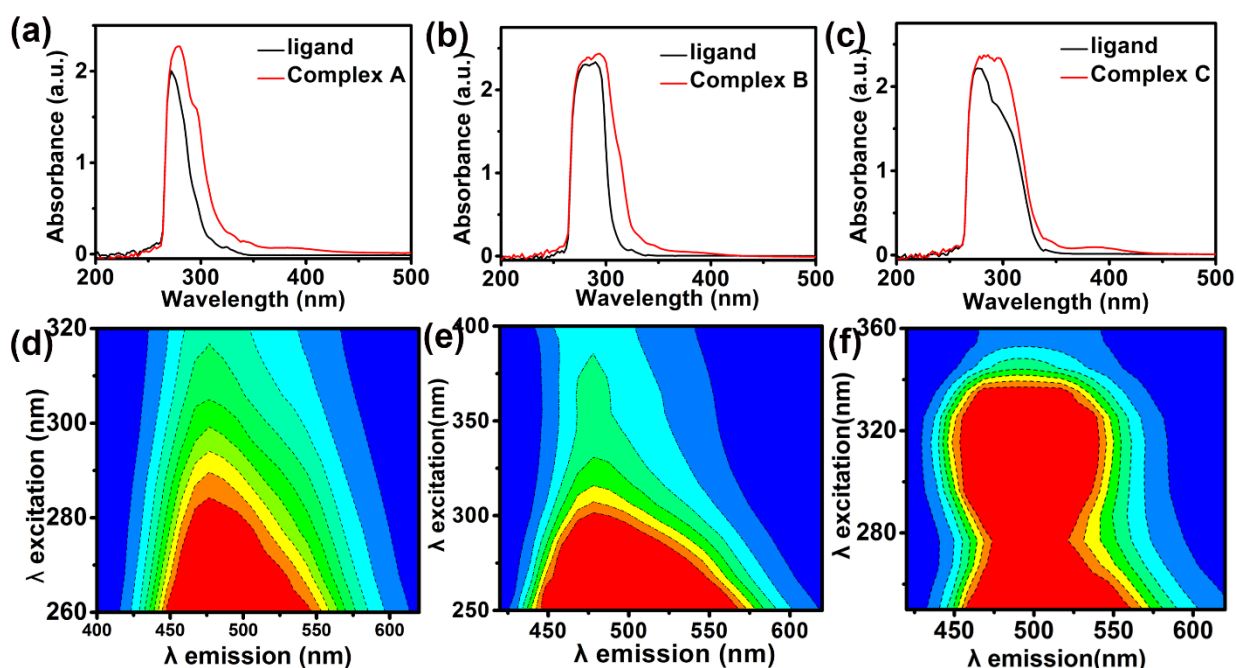


Figure 7. UV–visible absorptions of (a) benzylimidazole and its copper (II) Complex A, (b) bipyridine and its copper (II) Complex B, (c) salicylic acid and its copper (II) Complex C, and 2-dimensional excitation–emission spectra of (d) Complex A, (e) Complex B, and (f) Complex C.

Figure 7d–f illustrates the two-dimensional excitation–emission correlations. Excitation on the vertical axis corresponds to absorption spectra in Figure 7a–c for each copper (II) complex. Hence, vertical slices at strong emission wavelengths in Figure 7d–f yield the absorption spectra in Figure 7a–c. Emission wavelengths on the horizontal axis are given as a function of the excitation wavelength. Fluorescent intensity contours increase from dark blue (i.e., zero) to red (i.e., maximum) [14].

The fluorescent emission of important undiluted ligands and all three copper (II) complexes in DMF at an ambient temperature is illustrated in Figure 8a–e. In each case, excitation induces a π - π^* transition in the ligand, with subsequent ligand-to-metal energy transfer in the copper (II) complexes. A higher intensity emission occurs at longer wavelengths in all copper (II) complexes (i.e., red curves) relative to the emission in the corresponding undiluted ligands (i.e., black curves), according to Figure 8a–c. Results corresponding to the excitation and maximum emission intensity for three copper (II) complexes are summarized as follows:

Benzylimidazole; excitation = 280 nm, ligand emission = 400 nm, copper (II) complex emission = 468 nm

Bipyridine; excitation = 294 nm, ligand emission = 425 nm, copper (II) complex emission = 485 nm

Salicylic acid; excitation = 286 nm, ligand emission = 390 nm, copper (II) complex emission = 473 nm

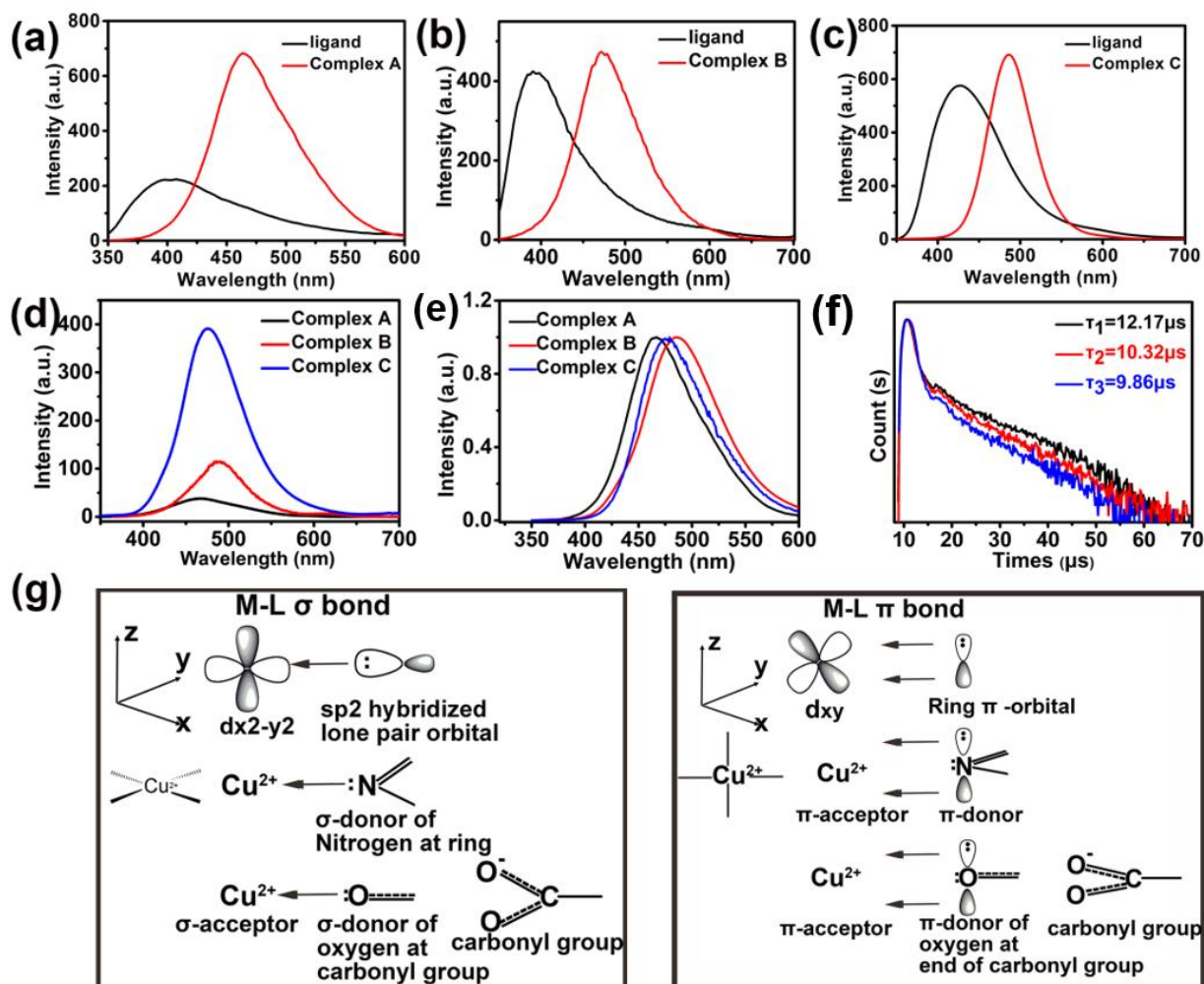


Figure 8. Fluorescence emission spectra for (a) benzylimidazole and its copper (II) Complex A (slit width = 20×20), (b) bipyridine and its copper (II) Complex B (slit width = 20×20), (c) salicylic acid and its copper (II) Complex C (slit width = 10×10), (d) comparison of luminescence intensity for all three copper (II) complexes (slit width = 10×10), (e) comparison of luminescence intensity for all three copper (II) complexes, each curve is normalized by its maximum intensity, (f) fluorescent decay curves for solid copper (II) complexes at the wavelength that corresponds to maximum emission intensity, and (g) molecular orbitals for copper (II) complexes subjected to Jahn–Teller distortions.

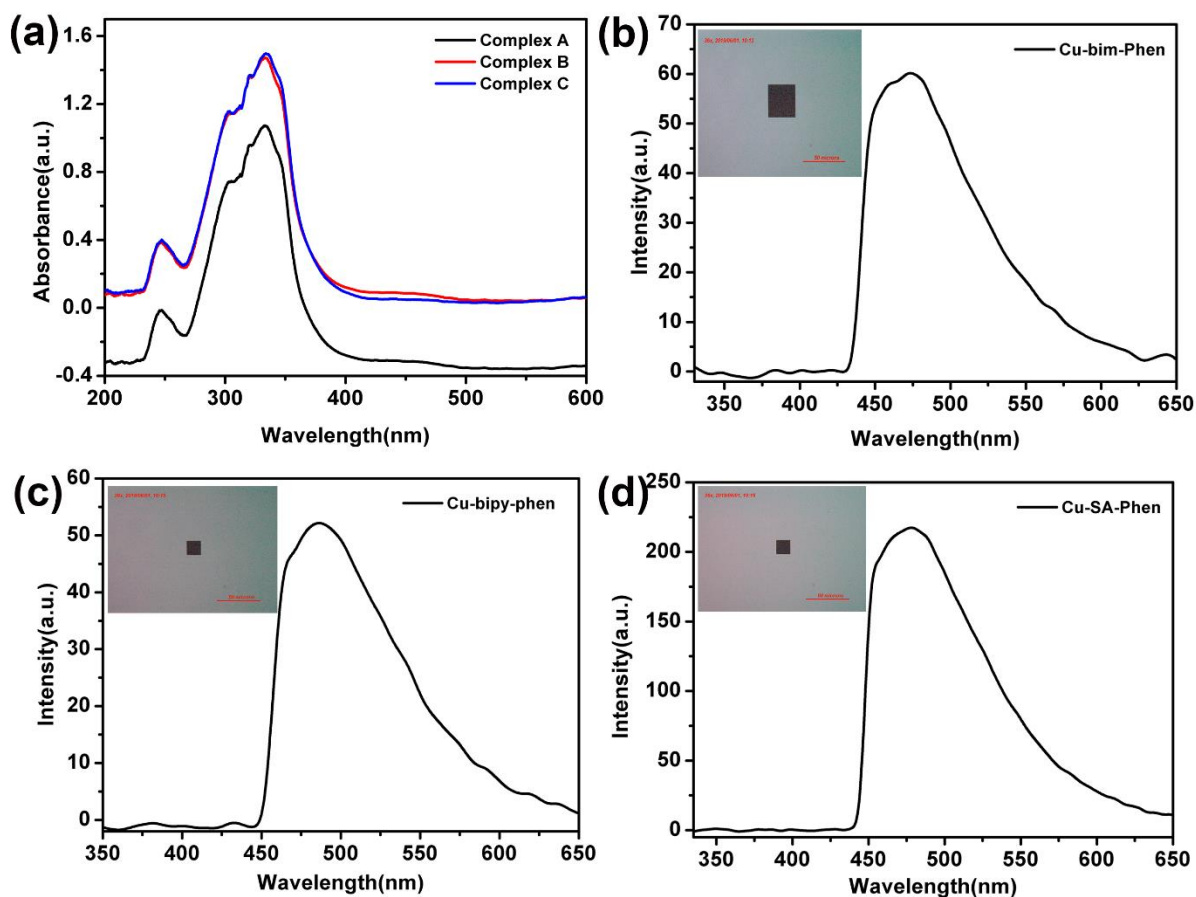
Slit-width-corrected luminescent data in Figure 8d reveal that copper (II) complexes with salicylic acid exhibit at least a 4-fold increase in emission relative to the corresponding complexes with bipyridine or benzylimidazole, suggesting that copper (II) complexes with salicylic acid represent excellent candidates for photoactive materials that emit blue-green light. Figure 8f and Table 3 summarizes transient fluorescent decays, lifetimes, and quantum yields for all three copper (II) complexes in the solid state at an ambient temperature, in response to excitation at 306 nm.

Table 3. Quantum yields and phosphorescence lifetimes of solid Cu²⁺ complexes.

Copper (II) Complex	Copper (II) Complex Structure	Quantum Yield (%)	Phosphorescence Lifetime (μs)	Emission Wavelength (nm)
A	Cu(bim)2(phen)	1.5	12.2	468
B	Cu(bipy)(phen)	4.9	10.3	485
C	Cu(SA)(phen)	11.9	9.9	473

Copper (II) complexes with salicylic acid exhibit the highest quantum yield, considering all three copper (II) complexes in this investigation (i.e., see Table 3) and all five copper (II) complexes studied previously (i.e., see Table 1). It is postulated that the sigma-donor and pi-donor characteristics of the carboxylic acid group in salicylic acid are responsible for efficient photo-emissions [38].

As shown in Figure 9, the absorption of the desired solid powder and the solid luminescence are given. In Figure 9a, the absorption range is not very different and is very similar. In Figure 9b,c, the solid luminescence and color pictures of the Complex A, B, and C powders are given. The wavelength of the complex emission and the color of the luminescence can be visually observed. In addition, by measuring the quantum yield of solid powder, we can find that the yield is C (30.75%) > B (13.35%) > A (6.8%). The powder precipitates in the liquid, and the concentration of the solid powder is increased, so the quantum yield is increased.

**Figure 9.** The absorption of all three copper (II) complexes (a) and solid luminescence of the copper (II) complexes with (b) benzylimidazole, (c) bipyridine, and (d) salicylic acid.

To further study the effect of Cu²⁺ content on the luminescence intensity of complexes, we changed the concentration of Cu²⁺ ions in each complex, and the results are shown in

Figure 10a–c. It is noticeable that as the concentration increases, the luminescence intensity increases firstly, and then decreases. The complexes showed the strongest luminescence intensity when the concentration of Cu^{2+} was 0.02 mol/L. Excessive Cu^{2+} content causes the distance between centers to become a less than critical distance, which will produce a cascading energy transfer until finally entering an annihilation center to cause an energy transfer, which results in the annihilation of luminescence.

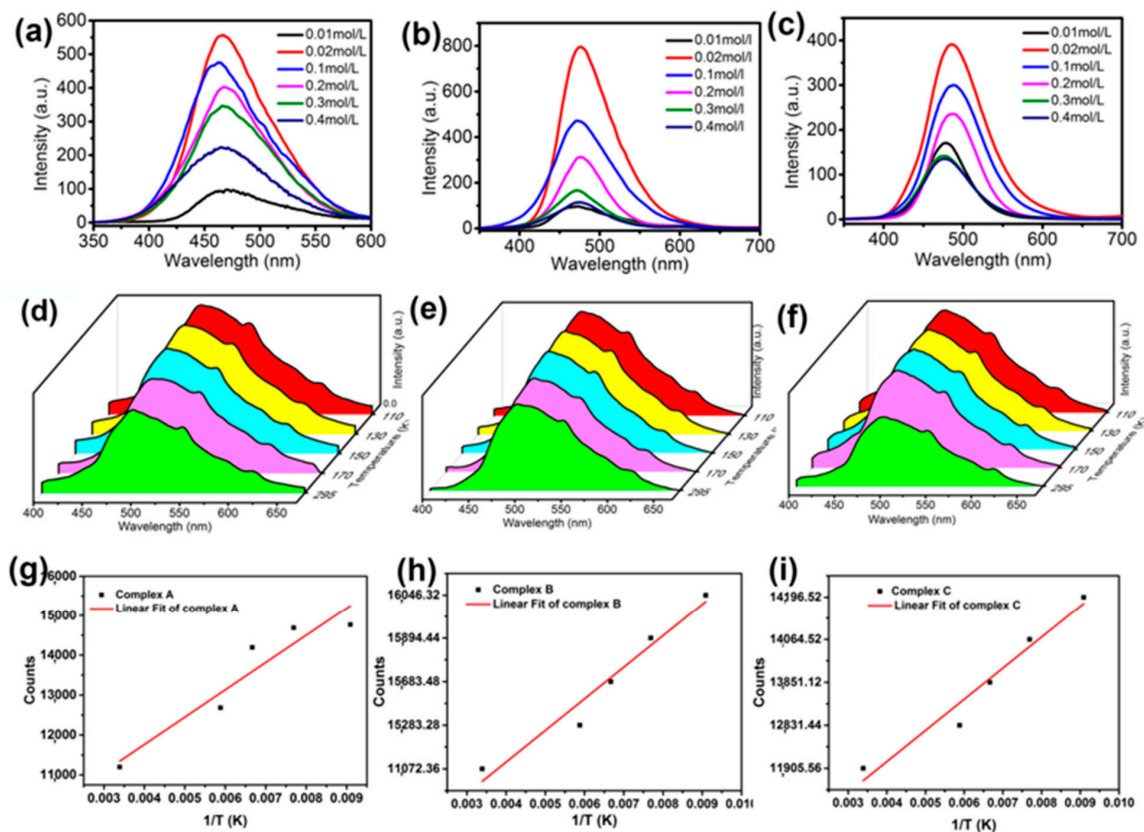


Figure 10. Concentration-dependent fluorescent emission in DMF at ambient temperature for copper (II) complexes with (a) benzylimidazole, (b) bipyridine, and (c) salicylic acid. Temperature-dependent fluorescent emission, between 110 K and 295 K for copper (II) complexes with (d) benzylimidazole, (e) bipyridine, and (f) salicylic acid. (g–i) Effect of temperature on maximum fluorescent intensity.

We also investigated the temperature influence on the emission of Cu^{2+} complexes from room temperature (295 K) down to 110 K. The temperature range is over a 185 K difference. As can be seen in Figure 10d–f, with the increase in temperature, the luminescent intensities exhibit a slight decline in intensity. On the other hand, there is a small, but apparent, spectral shift of the emission data upon decreasing the temperature. This phenomenon is generally expected for low-temperature experiments, resulting from thermal effects. At a low temperature, the Cu^{2+} atomic and ligand molecular thermal vibrations decreased and the ion-ligand aggregations became more condensed. All these occurrences cause less excitation energy loss and, thus, behave as a gradual blue-shift and a sharpening of the emission features. Based on the Figure 10g–i, we can try to simulate the data into a common equation, as follows:

$$I(T) = I_0 + \frac{A}{T} \quad (1)$$

where T is the absolute temperature (K), $I(T)$ is temperature-dependent luminescence intensity, and A is the temperature coefficient of luminescence intensity according to Equation (1), with dimensions of absolute temperature. Corresponding to Complex A, B, and C, this equation fits into the linear relationship in Figure 10g–i. The parameter values

of I_0 and A from the figures are listed in Table 4. R^2 is the correlation coefficient. Based on Equation (1), the luminescence intensity has a linear relationship with the reciprocal of the temperature.

Table 4. Parameters for temperature-dependent luminescence, according to Equation (1).

Complex	I_0	A (Kelvin)	R^2
A = copper (II) with benzyimidazole	5.38	−638	0.87
B = copper (II) with bipyridine	7.7	−720	0.90
C = copper (II) with salicylic acid	7.74981	−725.82	0.945

3.3. TG and Electrochemistry

The thermogravimetric analysis of complexes was carried out in the range of 18 °C to 900 °C in the presence of a nitrogen atmosphere with a heating rate of 10 °C min. As shown in Figure 11a, the initial mass loss of Complex A appeared at around 100 °C, which is mainly attributed to the evaporation of water molecules adsorbed at the surface of the complex. The major weight loss appeared at 230~500 °C range, which was caused by the pyrolysis of ligands sheets. For the coordination polymers B and C, there was no strictly clean weight loss step that occurred below 320 °C. The framework collapse and a sharp decomposition took place (a weight loss of 55%) from 320 to 600 °C, which can be assigned to the loss of ligands and phen [39–41]. The above-mentioned weight loss occurs later than in Complex A and it clearly proves that the thermal stability of complexes is in the order of $C > B > A$.

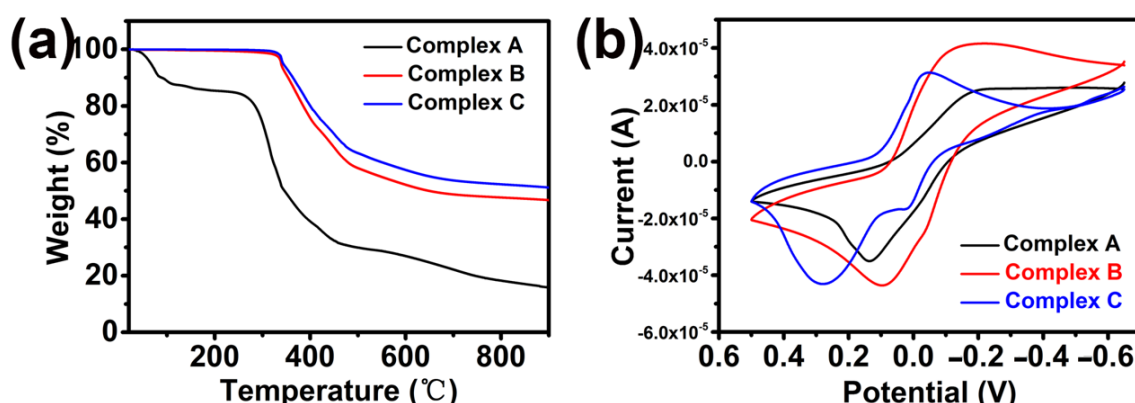


Figure 11. Illustrations of the (a) TG of the complexes and (b) cyclic voltammogram of complexes in KCl (solution 0.1 M) at 273 K using a glassy carbon working electrode, platinum wire auxiliary electrode, and an Ag/AgCl reference electrode; scan rate 100 mVs^{−1}.

The electrochemical properties of the copper complexes were studied by cyclic voltammetry (CV). The voltammogram of complexes is shown in Figure 11b. Three complexes were redox active and displayed a quasi-reversible cyclic voltametric response. The voltammogram of the Cu²⁺ complexes indicated only one single reduction peak (Cu²⁺/Cu⁺) for each complex during the cathodic potential scan, which is located at −0.216 V, −0.212 V, and −0.048 V, respectively. During the return anodic potential scan, just after the reduction peak, an anodic peak is observed at 0.136, 0.097, and 0.278 V, respectively. The separation between the cathodic and anodic peak potentials ΔE_p ($\Delta E = E_{pa} - E_{pc}$) of 180 mV indicate a quasi-reversible redox process assignable to the Cu(II)/Cu(I) couple, and $E_{1/2}$ [($E_{pa} + E_{pc}$)/2] is equal to −0.095, 0.0575, and 0.115 V, respectively. The redox potential [$A (-0.095) < B (0.0575) < C (0.115)$] is attributed to the extension of the corresponding π framework around the Cu²⁺ center.

4. Conclusions

In conclusion, Cu²⁺ complexes were synthesized and characterized by FTIR, XPS, ¹H NMR, UV-absorption, and luminescence emission. Luminescence studies of all three copper (II) complexes revealed blue-green emissions in each case. The highest quantum yield in DMF is achieved for copper (II) complexes with salicylic acid. Three ligands and their copper (II) complexes exhibited ambient-temperature luminescence, suggesting that these materials could be useful for luminescent devices. An increase in the concentration of copper (II) complexes in DMF reveals that maximum fluorescent emission occurs at 0.02 mole/Liter, prior to the onset of luminescence annihilation at higher copper (II) concentrations. There was a small but prominent spectral shift in the emission data upon decreasing the temperature that is generally expected for low-temperature experiments, resulting from thermal effects, including temperature-dependent solvent reorganization effects, causing a gradual blue-shift and a sharpening of the emission features. According to the literature, the UV–Vis absorption range of β-carotene is in the range of 400–550 nm, which is just within the range of the three complexes. Therefore, the complex solution can be made into a film, so that the luminescence is absorbed by β-carotene and, theoretically, the content of β-carotene can be increased, resulting in an increase in the yield of the carrot. After three months of observation on the synthesized copper complexes, the copper complexes have good chemical stability, the structure and the appearance remain unchanged, and the emission is stable. The complexes will have good application prospects in the fields of agriculture and marine science.

Author Contributions: Conceptualization, J.W., J.R., Z.D., L.H. and J.T.; methodology, J.W. and J.R.; validation, J.W., J.R., Q.T. and X.W.; formal analysis, J.W., W.W. and J.R.; investigation, X.W.; resources, Y.W. (Yao Wang), Y.W. (Yanxin Wang) and Q.T.; writing—original draft preparation, J.W.; writing—review and editing, J.W. and J.R.; visualization, J.T. and W.W.; supervision, J.T.; project administration, L.A.B.; funding acquisition, J.T. All authors have read and agreed to the published version of the manuscript.

Funding: This work was supported by (1) National Science Foundation of China (51473082), (2) State Key Project of International Cooperation Research (2017YFE0108300, 2016YFE0110800); (3) The Program for Introducing Talents of Discipline to Universities (“111” plan); (4) The double hundred foreign expert project of Shandong Province (2018–2021); (5) 1st class discipline program of Materials Science of Shandong Province.

Data Availability Statement: All data, models, and code generated or used during the study appear in submitted article.

Conflicts of Interest: The authors declare no conflict of interest.

References

1. Napierala, S.; Walesa-Chorab, M. On-substrate postsynthetic metal ion exchange as a tool for tuning electrochromic properties of materials. *Eur. Polym. J.* **2020**, *140*, 110052. [[CrossRef](#)]
2. Artem'ev, A.V.; Davydova, M.P.; Berezin, A.S.; Brel, V.K.; Morgalyuk, V.P.; Bagryanskaya, I.Y.; Samsonenko, D.G. Luminescence of the Mn²⁺ ion in non-O-h and T-d coordination environments: The missing case of square pyramid. *Dalton Trans.* **2019**, *48*, 16448–16456. [[CrossRef](#)] [[PubMed](#)]
3. Berezin, A.S.; Davydova, M.P.; Bagryanskaya, I.Y.; Artyushin, O.I.; Brel, V.K.; Artem'ev, A.V. A red-emitting Mn(II)-based coordination polymer build on 1,2,4,5-tetrakis (diphenylphosphinyl)benzene. *Inorg. Chem. Commun.* **2019**, *107*, 107473. [[CrossRef](#)]
4. Bortoluzzi, M.; Castro, J.; Di Vera, A.; Palu, A.; Ferraro, V. Manganese(ii) bromo- and iodo-complexes with phosphoramidate and phosphonate ligands: Synthesis, characterization and photoluminescence. *New J. Chem.* **2021**, *45*, 12871–12878. [[CrossRef](#)]
5. Zhang, S.; Zhao, Y.; Zhou, J.; Ming, H.; Wang, C.-H.; Jing, X.; Ye, S.; Zhang, Q. Structural design enables highly-efficient green emission with preferable blue light excitation from zero-dimensional manganese (II) hybrids. *Chem. Eng. J.* **2021**, *421*, 129886. [[CrossRef](#)]
6. Banasz, R.; Walesa-Chorab, M. Polymeric complexes of transition metal ions as electrochromic materials: Synthesis and properties. *Coord. Chem. Rev.* **2019**, *389*, 1–18. [[CrossRef](#)]
7. El-Habeeb, A.A.; Refat, M.S. Synthesis, structure interpretation, antimicrobial and anticancer studies of tranexamic acid complexes towards Ga(III), W(VI), Y(III) and Si(IV) metal ions. *J. Mol. Struct.* **2019**, *1175*, 65–72. [[CrossRef](#)]

8. Loncarevic, A.; Ivankovic, M.; Rogina, A. Electrospayed Chitosan-Copper Complex Microspheres with Uniform Size. *Materials* **2021**, *14*, 5630. [[CrossRef](#)]
9. Ma, D.L.; Wong, S.Y.; Kang, T.S.; Ng, H.P.; Han, Q.B.; Leung, C.H. Iridium(III)-based chemosensors for the detection of metal ions. *Methods* **2019**, *168*, 3–17. [[CrossRef](#)]
10. Adnan, S.; Al-Adilee, K.J.; Abedalrazaq, K.A. Synthesis, Spectral Characterization And Anticancer Studies of Novel Azo Schiff Base And its Complexes with Ag(I), Au(III) And Pt(IV) ions. *Egypt. J. Chem.* **2020**, *63*, 4749–4756.
11. Bharadwaj, N.; Kaushik, J. Comparative Study of Complexation of Midodrine Hydrochloride and Noradrenaline with Ag (I) Metal Ion—A Spectroscopic Method. *Int. J. Life Sci. Pharma Res.* **2020**, *10*, L53–L56.
12. Chen, W.C.; Sukpattanachoen, C.; Chan, W.H.; Huang, C.C.; Hsu, H.F.; Shen, D.; Hung, W.Y.; Kungwan, N.; Escudero, D.; Lee, C.S.; et al. Modulation of Solid-State Aggregation of Square-Planar Pt(II) Based Emitters: Enabling Highly Efficient Deep-Red/Near Infrared Electroluminescence. *Adv. Funct. Mater.* **2020**, *30*, 2002494. [[CrossRef](#)]
13. Kryuchkova, N.A.; Mironov, I.V.; Afanas'eva, V.A. The effect of ligand modification on the structure and electronic spectra of tetraazamacrocyclic complexes Au(III). *J. Mol. Struct.* **2021**, *1224*, 129162. [[CrossRef](#)]
14. Chabera, P.; Liu, Y.; Prakash, O.; Thyraug, E.; El Nahhas, A.; Honarfar, A.; Essen, S.; Fredin, L.A.; Harlang, T.C.B.; Kjaer, K.S.; et al. A low-spin Fe(III) complex with 100-ps ligand-to-metal charge transfer photoluminescence. *Nature* **2017**, *543*, 695–699. [[CrossRef](#)] [[PubMed](#)]
15. McCusker, C.E.; Castellano, F.N. Design of a Long-Lifetime, Earth-Abundant, Aqueous Compatible Cu(I) Photosensitizer Using Cooperative Steric Effects. *Inorg. Chem.* **2013**, *52*, 8114–8120. [[CrossRef](#)]
16. Nnabuike, G.G.; Salunke-Gawali, S.; Patil, A.S.; Butcher, R.J.; Lawal, M.; Bamigboye, M.O.; Obaleye, J.A. Copper(II) and Nickel(II) complexes of the non-steroidal anti-inflammatory drug indomethacin containing aromatic chelating N,N-donor ligand: Synthesis and structural studies. *J. Mol. Struct.* **2021**, *1224*, 129069. [[CrossRef](#)]
17. Padnya, P.; Shibaeva, K.; Arsenyev, M.; Baryshnikova, S.; Terenteva, O.; Shiabiev, I.; Khannanov, A.; Boldyrev, A.; Gerasimov, A.; Grishaev, D.; et al. Catechol-Containing Schiff Bases on Thiocalixarene: Synthesis, Copper (II) Recognition, and Formation of Organic-Inorganic Copper-Based Materials. *Molecules* **2021**, *26*, 2334. [[CrossRef](#)]
18. Tang, H.; Zhou, Z.; Li, Z.; Chen, S.; Wang, L.; Zhang, T. Copper (II) complexes of 1-methyl-5-aminotetrazole with different energetic anions: Syntheses, crystal structures and properties. *J. Energetic Mater.* **2021**, *39*, 23–32. [[CrossRef](#)]
19. Li, L.; Huang, M.; Liu, X.H.; Sun, D.M.; Shao, C.Y. In Situ Generation of Fluorescent Copper Nanoclusters Embedded in Monolithic Eggshell Membrane: Properties and Applications. *Materials* **2018**, *11*, 1913. [[CrossRef](#)]
20. Devi, L.R.; Raza, M.K.; Musib, D.; Ramu, V.; Devi, J.; Roy, M. Nucleus targeting anthraquinone-based copper (II) complexes as the potent PDT agents: Synthesis, photo-physical and theoretical evaluation. *Inorg. Chim. Acta* **2020**, *500*, 119208. [[CrossRef](#)]
21. Kumar, P.; Kumar, V.; Kaur, N.; Mobin, S.M.; Kaur, P.; Singh, K. A fluorene based probe: Synthesis and “turn-on” water sensitivity of the in-situ formed Cu²⁺ complex: Application in bio-imaging. *Anal. Chim. Acta* **2022**, *1189*, 339211. [[CrossRef](#)] [[PubMed](#)]
22. Wang, Z.G.; Chen, B.K.; Rogach, A.L. Synthesis, optical properties and applications of light-emitting copper nanoclusters. *Nanoscale Horiz.* **2017**, *2*, 135–146. [[CrossRef](#)] [[PubMed](#)]
23. Bencini, A.; Lippolis, V. 1,10-Phenanthroline: A versatile building block for the construction of ligands for various purposes. *Coord. Chem. Rev.* **2010**, *254*, 2096–2180. [[CrossRef](#)]
24. Walger, E.; Marlin, N.; Molton, F.; Mortha, G. Study of the Direct Red 81 Dye/Copper(II)-Phenanthroline System. *Molecules* **2018**, *23*, 242. [[CrossRef](#)] [[PubMed](#)]
25. Feng, Y.; Wang, L.; Xing, Z.; Huang, Q.; Ma, P. A new Cu(II) coordination polymer constructed from two kinds of ligands and rare Ta2OF10 (2-) anion: Synthesis, crystal structure and fluorescent properties. *Inorg. Chem. Commun.* **2018**, *93*, 15–19. [[CrossRef](#)]
26. Zang, Q.; Zhong, G.-Q.; Wang, M.-L. A copper(II) complex with pyridine-2,6-dicarboxylic acid: Synthesis, characterization, thermal decomposition, bioactivity and interactions with herring sperm DNA. *Polyhedron* **2015**, *100*, 223–230. [[CrossRef](#)]
27. Kim, H.T.; Kang, E.; Kim, M.; Joo, J.M. Synthesis of Bidentate Nitrogen Ligands by Rh-Catalyzed C-H Annulation and Their Application to Pd-Catalyzed Aerobic C-H Alkenylation. *Org. Lett.* **2021**, *23*, 3657–3662. [[CrossRef](#)]
28. Radhika, S.; Aneesa, T.; Philip, R.M.; Anilkumar, G. Recent advances and trends in the biomimetic iron-catalyzed asymmetric epoxidation. *Appl. Organomet. Chem.* **2021**, *35*, e6217. [[CrossRef](#)]
29. Zhang, W.C.; Lu, X. Long-lived photoluminescence and high quantum yield of copper(II) complexes with novel nanostructures. *Rsc Adv.* **2015**, *5*, 101155–101161. [[CrossRef](#)]
30. Yamgar, B.A.; Sawant, V.A.; Jadhav, A.N.; Chavan, S.S. Synthesis, characterization and photoluminescence properties of copper(II)-azido/thiocyanato complexes with thiazolylazo dye and 1,2-bis(diphenylphosphino)ethane. *Inorg. Chem. Commun.* **2010**, *13*, 1207–1209. [[CrossRef](#)]
31. Bibi, S.; Mohamad, S.; Manan, N.S.A.; Ahmad, J.; Kamboh, M.A.; Khor, S.M.; Yamin, B.M.; Halim, S.N.A. Synthesis, characterization, photoluminescence, and electrochemical studies of novel mononuclear Cu(II) and Zn(II) complexes with the 1-benzylimidazolium ligand. *J. Mol. Struct.* **2017**, *1141*, 31–38. [[CrossRef](#)]
32. Su, S.; Cheng, M.-I.; Ren, Y.; Zhai, C.; Tao, F.; Liu, Q. Three transition metal complexes with uncoordinated carboxyl groups: Synthesis, structures, and luminescence properties. *Transit. Met. Chem.* **2014**, *39*, 559–566. [[CrossRef](#)]
33. Alwis, D.D.D.H.; Chandrika, U.G.; Jayaweera, P.M. Spectroscopic studies of neutral and chemically oxidized species of beta-carotene, lycopene and norbixin in CH₂Cl₂: Fluorescence from intermediate compounds. *J. Lumin.* **2015**, *158*, 60–64. [[CrossRef](#)]

34. Martin, H.J.; Schulz, K.H.; Bumgardner, J.D.; Walters, K.B. XPS study on the use of 3-aminopropyltriethoxysilane to bond chitosan to a titanium surface. *Langmuir* **2007**, *23*, 6645–6651. [[CrossRef](#)]
35. Lawrie, G.; Keen, I.; Drew, B.; Chandler-Temple, A.; Rintoul, L.; Fredericks, P.; Grondahl, L. Interactions between alginate and chitosan biopolymers characterized using FTIR and XPS. *Biomacromolecules* **2007**, *8*, 2533–2541. [[CrossRef](#)]
36. Xiang, Y.; Zhang, Q.; Si, J.; Du, J.; Guo, H.; Zhang, T. Characterization and catalytic kinetics studies of N-cetyl-O-sulfate chitosan multinuclear copper complex as an artificial hydrolase. *J. Mol. Catal. A-Chem.* **2010**, *322*, 33–38. [[CrossRef](#)]
37. Anitha, C.; Sheela, C.D.; Tharmaraj, P.; Raja, S.J. Synthesis and characterization of VO(II), Co(II), Ni(II), Cu(II) and Zn(II) complexes of chromone based azo-linked Schiff base ligand. *Spectrochim. Acta Part A-Mol. Biomol. Spectrosc.* **2012**, *98*, 35–42. [[CrossRef](#)]
38. Chowdhury, S.; Bhattacharya, A.; Saha, P.; Majumder, S.; Suresh, E.; Naskar, J.P. A copper(II) complex of benzimidazole-based ligand: Synthesis, structure, redox aspects and fluorescence properties. *J. Coord. Chem.* **2016**, *69*, 3664–3676. [[CrossRef](#)]
39. Mondragon, M.; Elizalde, L.E.; Gomez-Vidales, V.; Arias, E.; Moggio, I. Luminescent copper(I, II) complex-anchored halloysite clay nanotubes. *Mater. Chem. Phys.* **2018**, *212*, 237–244. [[CrossRef](#)]
40. Tian, D.; Liu, X.-J.; Chen, R.-Y.; Zhang, Y.-H. Syntheses, structures, luminescent and magnetic properties of two coordination polymers based on a flexible multidentate carboxylate ligand. *Chin. Chem. Lett.* **2015**, *26*, 499–503. [[CrossRef](#)]
41. Pavlishchuk, A.V.; Kolotilov, S.V.; Zeller, M.; Thompson, L.K.; Addison, A.W. Formation of Coordination Polymers or Discrete Adducts via Reactions of Gadolinium(III)-Copper(II) 15-Metallacrown-5 Complexes with Polycarboxylates: Synthesis, Structures and Magnetic Properties. *Inorg. Chem.* **2014**, *53*, 1320–1330. [[CrossRef](#)] [[PubMed](#)]